Appl Phys B (2011) 103:917–924
DOI 10.1007/s00340-010-4287-0

Applied Physics B
Lasers and Optics

High efficiency dye laser with low fluorescence yield pyrromethene dyes: experimental and theoretical studies

K.K. Jagtap · D.K. Maity · A.K. Ray · K. Dasgupta · S.K. Ghosh

Received: 4 September 2010 / Revised version: 24 September 2010 / Published online: 6 November 2010

Abstract A combined experimental and theoretical study of the photo-physical, laser properties and molecular structures of three relatively recent Pyrromethene (PM) class dyes, PM597, PM580 and PM567, have been carried out. Laser characteristics of these three PM dyes were compared with three other widely used Rhodamine (RH) class dyes, RH6G, RHB and KRS, using a narrow-band dye laser setup, transversely pumped by the second harmonic (532 nm) of a Q-switched Nd-YAG laser. In addition to generating comparative data of these dyes for optimal use in dye lasers, we observed that unlike the RH dyes, the PM dyes show high efficiencies and wide tunability, despite the low fluorescence yield and high rate of non-radiative decay. Particularly, PM597 dye, in spite of a very low quantum yield of fluorescence ($\Phi = 0.42$), high non-radiative decay rate, and a large distortion from planarity in its excited state, when used in a laser cavity it exhibited similar laser efficiency and a beneficially wider tuning curve in comparison to other two PM dyes. Theoretical studies were carried out applying density functional theory and time-dependent density functional theory (DFT/TDDFT) to obtain new information on ground and the first excited state geometrical parameters of the PM dyes. Good correlation between calculated molecular properties and experimental results was observed for the evolution of the longest wavelength absorption maximum.

K.K. Jagtap · A.K. Ray (✉) · K. Dasgupta
Laser & Plasma Technology Division, Bhabha Atomic Research Centre, Mumbai 400085, India
e-mail: alokray@barc.gov.in

K.K. Jagtap
Chemistry Dept., Univ. of Pune, Pune 411007, India

D.K. Maity · S.K. Ghosh
Theoretical Chemistry Section Bhabha Atomic Research Centre, Mumbai 400085, India

D.K. Maity
e-mail: dkmaity@barc.gov.in

1 Introduction

Several chromophores of highly fluorescent organic compounds are now known, but the dipyrromethene BF_2 (PM or BODIPY) family of dyes has attracted interest over the past decade as being one of the more versatile fluorophores due to its applications as biomolecular labels [1], novel organic materials [2], fluorescent chemo-sensors [3], and active media in liquid [4] and solid-state [5] dye lasers, among others. The use of PMs as effective biological label has been complemented by their preference to function as an efficient laser dye. The general observation of good laser efficiency of PM dyes in solid-state as well as in liquid dye lasers has led to several investigations [6–8] on its photo-physical and laser properties. In parallel, more fundamental studies on the chemical reactivity and photo-degradation mechanism of the new PM dyes emerged. However, the rapid rate of photo-degradation of PM dyes in air-equilibrated liquid solutions, [9, 10] due to its self-sensitized photo-oxidation by reacting with generated singlet oxygen, remained a cause of primary concern for use in liquid dye lasers, especially in high-average power dye lasers. Remarkable improvement in the photo-stability of PM567 dye solutions, while deployed in low [9] as well as in high-repetition rate dye lasers [10], was observed with addition of 1,4-diazabicyclo [2,2,2] octane (DABCO), a singlet oxygen quencher. There have also been efforts [8, 12–14] to synthesize various analogues of PM dyes possessing better photo-stability as well as higher efficiency for dye laser and other applications.

Although photo-physical and laser characteristics of PM567 dye are widely studied, scanty reports are available for those [6] of PM580, and PM597 dye in liquid dye lasers and correlations of their photo-physical properties with molecular structures. Generally, a high quantum yield of fluorescence (Φ) and a small non-radiative rate of decay of the dye molecule in the solvent environment are prerequisites for high laser efficiency. The non-radiative deactivation processes are normally attributed to the rigidity/flexibility of the molecular structure of the chromophore. Additional processes that may affect net laser efficiency are ground-state absorption (GSA) and excited singlet–state absorption (ESA) at laser wavelengths, and these need to be accounted while considering the effect of molecular properties of dyes on their laser efficiencies. Therefore, a better understanding of correlations between molecular structures, photo-physical properties and laser efficiencies of available PM dyes is necessary to design modified PM dye molecules.

The present experimental and a time-dependent density functional theoretical investigations on PM597 and PM580 dyes, along with commonly studied PM567 dye, were taken up to generate supplementary information on their photophysical, laser properties and molecular parameters as well as the influence of the molecular structures on their properties. Herein, we report the results of our comprehensive investigations on laser performances of alcohol solutions of these Pyrromethene dyes, along with widely used Rhodamine 6G (RH6G), Rhodamine B (RHB) and Sulforhodamine B (KRS) dyes, using a narrow-band (∼0.1 cm^{-1}) dye laser set up, transversely pumped by the second harmonic (532 nm) of a Q-switched, pulsed (10 Hz) Nd-YAG laser. A significant observation was the efficient lasing performance of PM597 dye, comparable to PM580 and PM567 dyes and higher than RH dyes, despite poor photo-physical properties of the PM597 molecule [15]. Calculations of electronic structures of ground (S_0) and first excited (S_1) states of all three PM dyes were performed by time-dependent density functional theory (TDDFT) with appropriate long-range functional to understand the effect of the molecular structures on their photo-physics and hence, laser properties. Off late, it has been shown that by adding a long-range correction term [16–22] accounting for long-range exchange repulsions in the hybrid functional can improve excitation wavelengths significantly by eliminating overestimation of certain unphysical attraction terms. So, we have applied the formalism to calculate the excitation wavelengths. Theoretical studies establish that TDDFT (B3LYP)-PCM (Polarizable Continuum Model) combination is an excellent and reliable method for predicting the longest wavelength absorption maxima and other molecular data of PM dyes. It is demonstrated that reliable prediction of excited state properties of the dyes is possible and the method may be utilized in designing new PM dyes with desirable spectral properties for specific applications.

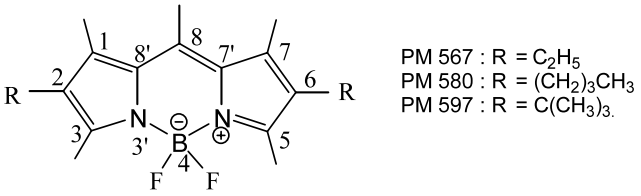

Fig. 1 Molecular structure of PM567, PM580 and PM597 dyes

2 Experimental methods

High purity laser grade dyes PM597, PM580 and PM567 were procured from Exciton and DABCO from Aldrich, and used as received. The molecular formula of all three PM dyes is shown in Fig. 1. Spectroscopy grade methanol and ethanol solvents were used to prepare dye solutions for this study. Absorption and steady-state fluorescence spectra of alcoholic PM dye solutions were recorded with commercial UV/VIS spectrophotometer (JASCO, V-550) and spectrofluorimeter (JASCO, FP-6500), respectively.

The measurement of quantum yield of fluorescence (Φ) of PM dyes was carried out using the comparative method of Williams et al. [23], ensuring linearity of fluorescence yield across the measured concentration range (1–3 × 10^{-6} M) of dye, which also validated the use of standard dye solution and its Φ value. PM567 was chosen as standard sample and it was cross calibrated with another dye, PM597. The time-resolved fluorescence measurements of dye solutions were carried out with a time-correlated single photon counting (TCSPC) set up from IBH, using a 490 nm LED (∼1.3 ns, 1 MHz repetition rate) as excitation source. Fluorescence decay curves were fitted as single-exponential decay and the fluorescence lifetime (τ) was calculated from the slope. All the measurements were performed at ambient temperature, the dye solutions being in equilibrium with the air.

Comparative studies of laser performances of PM and RH dye solutions were carried out by constructing a broad band as well as a narrow-band dye laser, transversely excited by 2nd harmonic of a Q-switched, pulsed (10 Hz) Nd-YAG laser, which have been described elsewhere [11]. Briefly, the narrow-band (line width ∼0.1 cm^{-1}) dye laser oscillator used an uncoated (4% reflectivity) output coupler and a grazing-incidence-grating (GIG) configuration (with a grating of 2400 lines/mm), with a (25X) 4-prisms pre-expander. To ensure similar gain depth for all dye solutions and provide a dye laser output with high efficiency and near-circular spatial profile, the concentrations of all dye solutions were optimized to have similar optical density at the pump wavelength, 532 nm. An optimized concentration of DABCO (∼100 mM) was added [11] to each air equilibrated PM dye solutions to reduce the rapid rate of photo-degradation of PM dyes. The tuning curve of each dye solution was obtained by rotation of the tuning mirror, and using an optical fiber coupled wave meter and an average power meter.

3 Theoretical methods

A search for the minimum energy structures in the ground (S_0) state of all the three PM dyes was carried out applying a correlated hybrid density functional, Becke's three parameter exchange augmented by Lee, Yang, and Parr's (B3LYP) using a Dunning-type correlation consistent atomic basis set, cc-pVDZ for all the atoms. A quasi Newton-Raphson based algorithm was applied to carry out geometry optimization for each of these dyes with various possible conformers as the initial structures. An electron correlated method, namely, time-dependent density functional theory (TDDFT) with B3LYP density functional was applied to study the excited state structure of the dyes in the first excited (S_1) state. Of late, different models have been proposed for long-range corrections in DFT functional replacing the DFT exchange part with the HF exchange to predict accurate excitation energies within time-dependent density functional formalism. Recently, density functional, PBE0 with long-range correction based on a modified exchange energy density (LRC-μPBE0) due to Hirao and co-workers [16–19] was also applied to find out the excited state energy parameters with the optimized geometry for the first excited state at TDDFT/B3LYP level of theory [20–22]. The value of the Coulomb attenuation parameter (μ) was taken as 0.33 in these excited state calculations. This DFT functional with long-range correction, LRC-μPBE0 was shown to predict accurate absorption spectra of organic dyes [24]. Note that Dunning-type correlation consistent atomic basis set, cc-pVDZ, was also used for all the excited state calculations. The ground (S_0) state minimum energy structures of these dyes, including PCM model with B3LYP functional, was searched by testing effect of macroscopic hydration. Excited state calculations are also carried out on these solvent modified geometries to determine the effect of solvent applying TDDFT with B3LYP functional coupled with PCM solvent model. All electronic structure calculations were carried out applying the GAMESS suite of ab initio program [25].

4 Results and discussion

4.1 Theoretical

Minimum energy structures of Pyrromethene dyes, PM567, PM580 and PM597 in the ground (S_0) and the first excited (S_1) states, applying B3LYP functional under DFT/TDDFT procedure including PCM solvent model, were computed and are displayed in Fig. 2 (i–iii). It is observed that the geometrical parameters in the ground state (S_0) are very close to that in the first excited state (S_1) in case of dyes PM567 and PM580 and the rings of the chromophore are almost planar. However, in case of dye PM597, the first excited state structure is largely distorted from planarity, as is evident from a large value of dihedral angle, $\angle C_2BC_8C_6 = 14.2°$. Also, a significant increase in the value of conjugation length, along the long molecular axis (C_2C_6), is observed for PM597 dye explaining red spectral shift of its absorption and emission spectra, in comparison to other two PM dyes. Selected geometrical parameters related to the chromophore of the three dyes in the ground and the first excited state based on DFT calculations are supplied in Table 1. A considerable modification in charge density of the atoms is observed in the first excited state compared to the ground state of PM dyes. The calculated atomic charges (in a.u.) of C(2), C(6), N(1), N(2), B, F(1) and F(2), atoms in S_0 state of dyes, based on B3LYP level calculation, and in the first excited state (S_1) at TD(B3LYP) level show significant electronic change, and these are tabulated in Table 2. Note that the two terminal carbon atoms at C(2) and C(6), along molecular axis, show positive atomic charges for the dye PM597, whereas negative charges are shown for PM567 and PM580 molecules.

Table 3 depicts calculated electronic transition wavelengths for the lowest transition; HOMO→LUMO at various levels of theory for all the three PM dyes and compares these values with the experimental data. It may be mentioned that the S_0–S_1 transition of PM dyes is a promotion of one electron from the HOMO to the LUMO state and it is polarized along the long molecular axis (C_2C_6), perpendicular to the molecular dipole moment. As seen from the table, vertical transitions are largely blue shifted at different levels of theory incorporating different DFT functional in TDDFT calculations in case of all the three dyes. Performance of long-range corrected DFT functional, namely LRC-μPBE0 under TDDFT formalism (method 2) is also poor in the present case and largely blue shifted by ∼90 nm, though it was shown earlier to produce accurate optical transition wavelengths with this particular DFT functional. Even application of a macroscopic model, such as a conductor-like polarizable continuum model (C-PCM), does not improve the calculated transition wavelengths. However, when the structures of the dyes are fully relaxed in the first excited state, the transition wavelengths improve significantly (see Method 4 in Table 3) toward the experimental values and these are much better than in an earlier theoretical report [8]. Surprisingly, the performance of LRC-μPBE0 functional is poor again when TDDFT calculation is repeated with this functional on relaxed structure of S_1 surface calculated at TDDFT(B3LYP) level of theory. Finally, we have carried out a single point excited state calculation including a PCM macroscopic solvation model on a relaxed S_1 surface without solvent effect (Method 6) and the values are listed in Table 3. These are the best-calculated transition wavelength values for the lowest electronic transitions, HOMO→LUMO in these three dyes. The HOMO orbital of the ground state and LUMO orbital of the first excited states are shown in Fig. 3. As can be noticed, participation of chromophore atoms B and F is minimal in both orbitals.

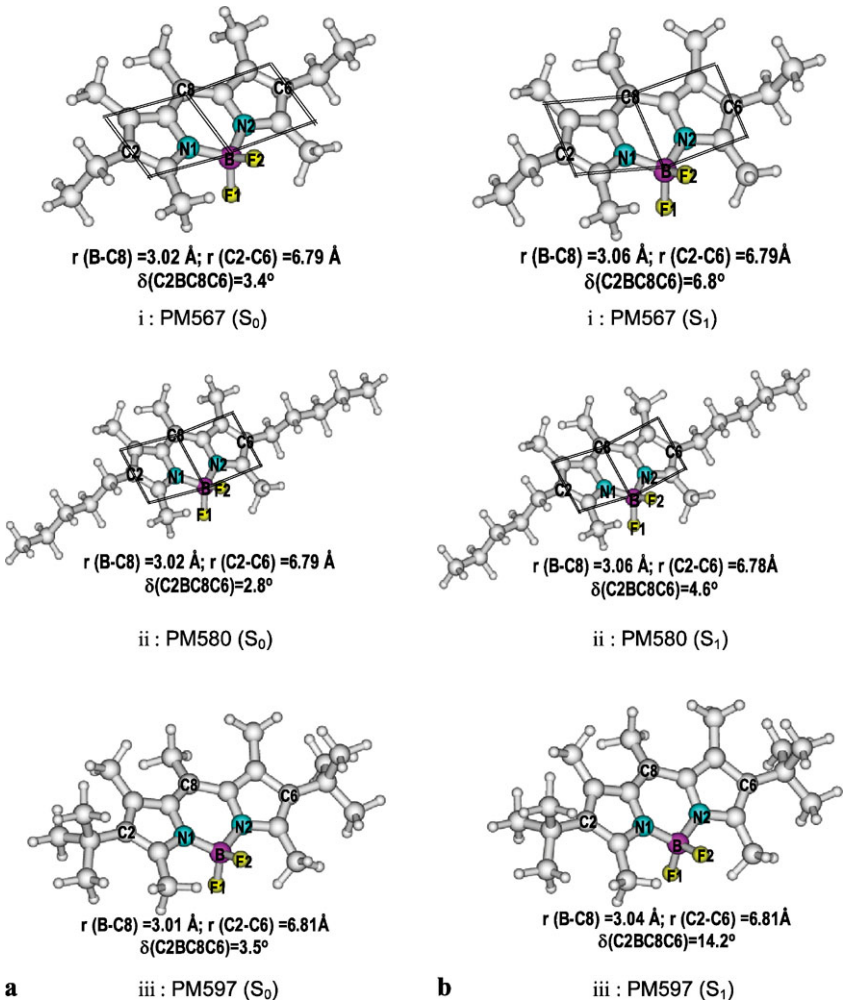

Fig. 2 Optimized structures in the (*i***a**) ground S_0 state and (*i***b**) first excited S_1 state of the dye PM567; (*ii***a**) ground S_0 state and (*ii***b**) first excited S_1 state of the dye PM580 and (*iii***a**) ground S_0 state and (*iii***b**) first excited S_1 state of the dye PM597. The ground state structures were optimized applying B3LYP/cc-pVDZ level of theory including C-PCM model. The excited state structures were optimized at TDDFT (B3LYP)/cc-pVDZ level of theory. Color codes: *yellow* for F atoms, *magenta* for B atoms, *blue* for N atoms and out of rest, smaller balls are for H atoms and larger balls are for C atoms

Table 1 Selected geometrical parameters of PM567, PM580 and PM597 dyes in the ground (S_0) and the first excited (S_1) states, calculated applying B3LYP and TD(B3LYP) methods, respectively, taking Dunning correlated atomic basis functions, cc-PVDZ for all the atoms

Dye	Pi-conjugation length for long axis (Å) (Top side)[a]		Pi-conjugation length for long axis (Å) (Bottom side)[a]		∠FBF (degree)		∠C2BC8C6 (degree)	
	Ground state (S_0)	First excited state (S_1)	Ground state (S_0)	First excited state (S_1)	Ground state (S_0)	First excited state (S_1)	Ground state (S_0)	First excited state (S_1)
PM567	8.501	8.598	8.629	8.619	109.5	109.3	3.4	6.8
PM580	8.504	8.585	8.634	8.617	109.6	109.6	2.8	4.6
PM597	8.521	8.627	8.667	8.674	109.8	109.9	3.5	14.2

[a]Top side refers to bond links: C2-C1-C8′-C8-C7′-C7-C6 (see Fig. 1) and bottom side refers to bond links: C2-C3-N3′-B4-N-C5-C6

4.2 Experimental

A typical illustration of observed linear fluorescence intensity plots for all three PM dyes in methanol solvent is shown in Fig. 4. The gradient of the plot for each dye solution is taken as proportional to the fluorescence quantum yield of that sample. Conversion into an absolute Φ is achieved using the equation:

$$\Phi_s = \Phi_r[\mathrm{Grad}_s/\mathrm{Grad}_r]\left[\eta_s^2/\eta_r^2\right]$$

where the subscripts 'r' and 's' denote reference and sample, respectively, 'Grad' the gradient from the plot of integrated fluorescence intensity vs. absorbance, and η is the refractive index of the solvent.

Table 2 Mulliken atomic charge density at atoms of PM chromophores

Atoms	Mulliken atomic charge on PM567 (a.u.)		Mulliken atomic charge on PM580 (a.u.)		Mulliken atomic charge on PM597 (a.u.)	
	Ground state (S_0)	First excited state (S_1)	Ground state (S_0)	First excited state (S_1)	Ground state (S_0)	First excited state (S_1)
C2	−0.067	−0.072	−0.067	−0.067	+0.059	+0.041
C6	−0.076	−0.120	−0.072	−0.113	+0.059	+0.059
N1	−0.21	−0.16	−0.21	−0.11	−0.20	−0.11
N2	−0.22	−0.15	−0.22	−0.11	−0.21	−0.11
B	0.21	0.02	0.19	0.0	0.18	0.03
F1	−0.24	−0.13	−0.23	−0.14	−0.22	−0.13
F2	−0.23	−0.14	−0.23	−0.13	−0.23	−0.13

Table 3 Comparison of calculated optical transition wavelength (λ) of PM567, PM580 and PM597 dyes with the experimental values. Time-dependent density functional theory (TDDFT) with functionals, B3LYP and PBE0 + long-range correction (LRC-μPBE0) are considered for the excited state calculations. Dunning correlated atomic basis functions, cc-PVDZ is adopted for all the atoms in these calculations

Theoretical method	Calculated λ(nm) for dye		
	PM567	PM580	PM597
Method1: TD(PBE0) (S_1)//B3LYP (S_0)	415	429	434
Method2: TD(LRC-μPBE0) (S_1)//B3LYP (S_0)	431	434	440
Method3: TD(B3LYP)+PCM (S_1)//B3LYP+PCM (S_0)*	439	441	441
Method4: TD(B3LYP) (S_1)//TD(B3LYP) (S_1)	539	515	575
Method5: TD(LRC-μPBE0) (S_1)//TD(B3LYP) (S_1)	454	458	467
Method6: TD(B3LYP)+PCM (S_1)//TD(B3LYP) (S_1)*	528	511	560
Experiment* (λ^a_{max})	518	519	523

*Ethanol solvent

Table 4 Photo-physical properties of PM and RH dyes in methanol and ethanol solvents

Dye	Solvent	λ^a_{max} (nm)	λ^e_{max} (nm)	ϵ^a_{max} (10^4 M^{-1} cm^{-1})	$\Delta\upsilon$ (cm^{-1})	Φ_f	τ (ns)	k_r (10^8 s^{-1})	k_{nr} ($10^8 s^{-1}$)
PM567	MeOH	516	535	7.9	688	0.84	6.37	1.31	0.251
PM567	EtOH	518	536	8.3	648	0.83	6.27	1.32	0.271
PM580	MeOH	517	537	7.5	721	0.86	6.23	1.38	0.224
PM580	EtOH	519	538	7.6	680	0.85	6.16	1.37	0.243
PM597	MeOH	522	562	7.3	1363	0.48	4.21	1.11	1.277
PM597	EtOH	523	564	7.4	1389	0.42	4.07	1.03	1.425
RH6G	EtOH	530	560	10.6*	1011	0.99#	4.5	2.17	0.04
RhB	EtOH	543	568	10.0+	811	0.7•	2.8	2.5	1.07
KRS	EtOH	555	574	11.9+	596	0.69•	3.8	1.82	0.82

Taken from references: (#) Ref. [26], (•) Ref. [28], (+) Ref. [27]

The measured photo-physical properties of PM and RH dye solutions, such as absorption maximum (λ^m_{abs}), fluorescence maximum (λ^m_{em}), fluorescence quantum yield (Φ) and fluorescence lifetime (τ) etc., are summarized in Table 4. It also includes values for radiative (k_r) and non-radiative (k_{nr}) rates of dyes, computed from the measured Φ and τ values. Photo-physical properties of both the PM567 and PM580 dyes show a close resemblance and these agree with the previously reported data [6, 12, 14]. The absorption and fluorescence spectra of PM597 dye were observed

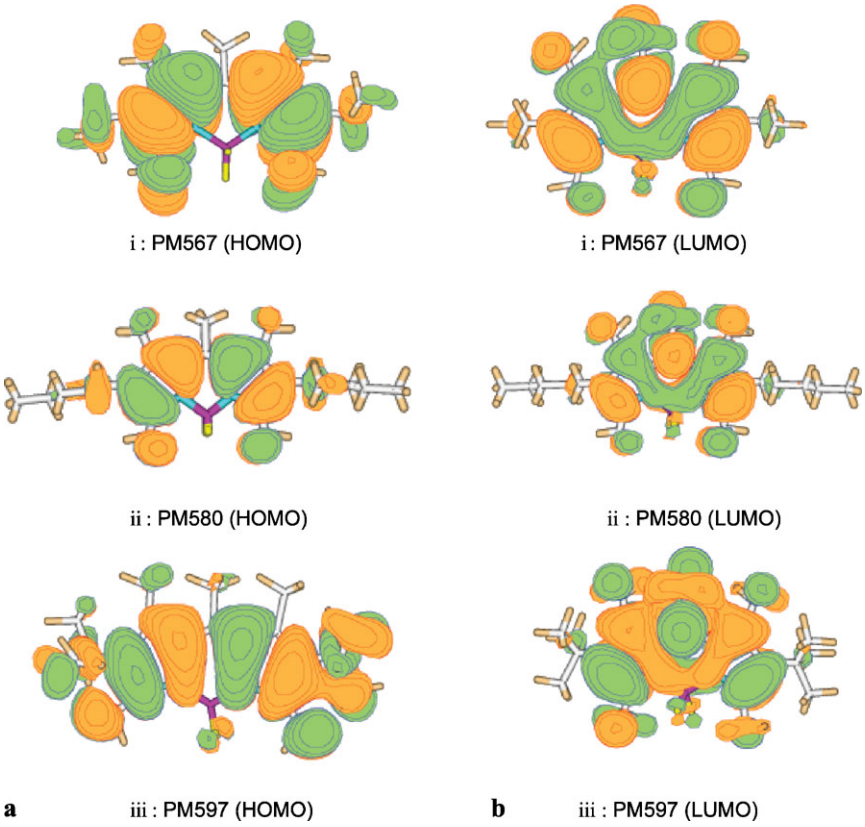

Fig. 3 Plot of (**a**) HOMO and (b) LUMO orbital in the ground S_0 state and the first excited S_1 state of the dye (*i*) PM567, (*ii*) PM580 and (*iii*) PM597 with the maximum contour value of 0.1

Table 5 Laser characteristics of PM567, PM580 and PM597 dye solutions

Dye	Solvent	Conc. of dye (mM)	Max. λ_L (nm)	Max. eff. η (%)	Threshold L_T (mJ)	Slope eff., η_s (%)	Tuning range (nm)
PM567	EtOH	0.88	558.3	23	0.3	24.1	546–580
PM567	MeOH	0.97	556.2	24	0.27	25.1	546–578
PM580	EtOH	0.71	557.7	22	0.35	23	548–580
PM580	MeOH	0.77	561	23	0.28	22.9	547–580
PM597	EtOH	0.28	575.1	20	0.45	22.1	561–611
PM597	MeOH	0.29	576	22	0.39	24.2	561–611
RH6G	EtOH	0.15	565	16.5	0.15	17.7	555–575
RhB[a]	EtOH	0.18	586	13.6	0.23	14.6	578–601
KRS[a]	EtOH	0.2	587	9.5	0.15	9.9	580–596

[a]Taken from Ref. [28]

to shift to longer wavelengths with respect to those of PM567 and PM580 dyes, which agrees with an earlier report [15]. However, the shift is much higher in the fluorescence (∼28 nm) than in the absorption (∼5 nm) spectra, and thus produced a large Stokes shift, $\Delta\upsilon$(∼1389 cm^{-1}). The large bathochromic shifts of absorption and particularly emission bands for PM597 originate from higher electron donating capability of the bulky alkyl groups at C2 and C6 carbon atom positions, which is substantially higher for *tert*-butyl groups in PM597 than for n-butyl groups in PM580 and ethyl groups in PM567. The electronic charge density at C2 and C6 carbon positions of the PM597 dye show positive values, in comparison to negative values for PM567 and PM580 (refer Table 2). Also, our calculation on geometrical parameters of the first excited state (S_1) of these dyes show dihedral angles (C2BC1C3) of 14.2° in the PM597 molecule, to be compared to 4.6° in PM580 and 6.8° in PM567. Thus, the observed large red shift in the fluorescence spectrum of dye PM597 is related to the enormous distortion of its excited (S_1) state from aromaticity, which, in turn, reduces the resonance energy of the emission band in the solvent environment. The observation of a considerably smaller fluorescence yield (Φ) and lifetime (τ) of PM597 dye is also related to the large dis-

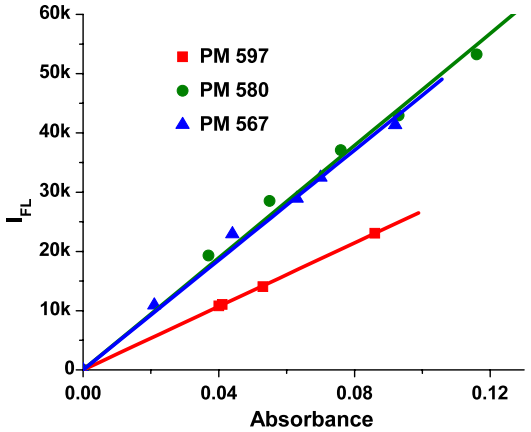

Fig. 4 Integrated Fluorescence Intensity (I_{FL}) Plot for (■) PM567, (●) PM580 and (▲) PM597 dyes using methanol solvent (PM567 and PM597 were considered as reference)

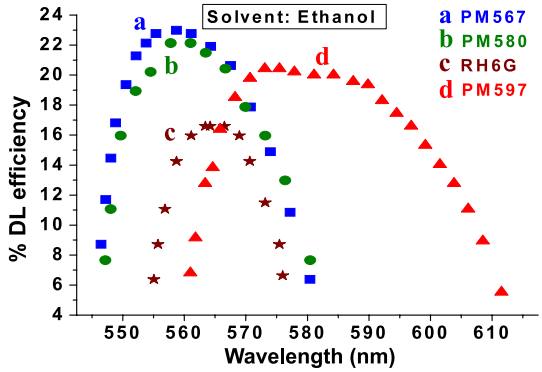

Fig. 5 Dye Laser (DL) tuning curves for (*a*) PM567, (*b*) PM580 and (*c*) PM 597 dyes using ethanol solvent. Pump wavelength: 532 nm, Pump energy ~7 mJ/pulse

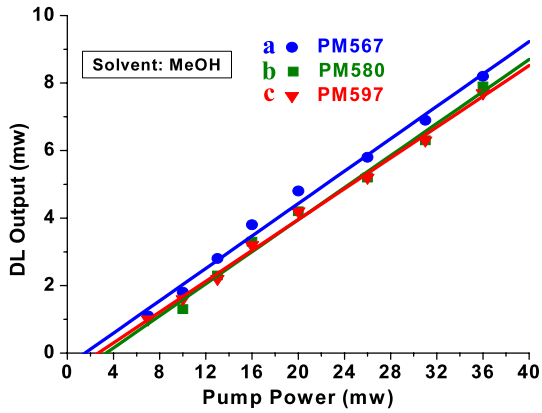

Fig. 6 Dye Laser (DL) gain curves of (*a*) PM567, (*b*) PM580 and (*c*) PM597 dyes using methanol as solvent at their respective peak laser wavelengths

torted geometry of PM597 from planarity in the excited state (S_1).

The observed narrow-band laser tuning curves for all three PM dyes using ethanol solvent, pumped by 532 nm of Nd-YAG laser, are shown in Fig. 5. PM567 and PM580 dyes produced laser gain in a similar region of spectra (545 nm to 580 nm) and had a comparable peak efficiency (~22%) at similar wavelengths (~558 nm). However, in concurrence with absorption and fluorescence spectra, the PM597 dye shows a lasing peak at significantly longer wavelength (578 nm) with wider tuning range: in the range of 560 nm to 610 nm. The methanol solvent based PM dyes produced marginally higher (1–2%) laser efficiency than that with ethanol, which correlates with slightly superior photophysical properties of these dyes in methanol (Table 4). The pump energy threshold (L_T) and slope efficiency (η_s) of each of the dye lasers at its respective peak laser wavelength were calculated by extrapolating the plot of dye laser power against pump power, which is illustrated for methanol solutions of PM dyes in Fig. 6. Table 5 summarizes laser properties of PM dyes, using both ethanol and methanol solvents. The corresponding data for RH dyes using ethanol solvent are also included for comparison. All the three PM dyes gave a substantially higher laser efficiency than even RH6G, the most efficient RH class dye. However, the RH6G dye laser produced a lower laser threshold, which was explained for PM567 and RH6G dyes using an analytical model in our earlier work [11]. The slightly lower peak (1–2%) lasing efficiency of PM597 dye was observed with respect to PM567 and PM580 dyes, using both the solvents. However, it is insignificant compared to the larger non-radiative rate (4.9 to 5.9 times) and smaller radiative rate (1.1 to 1.3 times) of PM597 dye in comparison to PM567 and PM580 dyes (Tables 4 and 5). This observation of high laser efficiency of PM597 dye, despite poor photo-physical properties, indicates that other mechanisms might be responsible.

The dye laser efficiency depends essentially on the net gain that depends, in turn, on radiative rate, non-radiative rate, ground and excited-state absorption (GSA, ESA) cross-sections at the laser wavelengths as well as on cavity losses and dynamic changes caused by time-dependent saturation of the gain. PM597 dye has shown a larger Stokes shift in fluorescence. Additionally, a lower concentration of dye PM597 (0.28 mM) was used in this study, on account of its higher absorption cross-section at the pump wavelength (532 nm). These two factors facilitated the reduction of GSA at lasing wavelengths of PM597, and in turn, the cavity losses for dye laser photons. A low ESA at laser wavelengths may also facilitate obtaining the high efficiency of PM597 dye. Rhodamine dyes are known [26] to have a significant ESA at the relevant laser wavelengths. It may be noted that our recent studies on high-repetition-rate (~6.3 kHz) dye lasers in oscillator-amplifier configuration, using ethanol solutions of PM567 and PM597 dyes with additive DABCO, carried out separately by pumping with green component (510 nm) of copper vapor lasers, show excellent photostability and efficiency of these PM dyes.

5 Conclusions

The superior laser performance of Pyrromethene (PM) dyes in comparison to Rhodamine (RH) dyes is clearly demonstrated. Comparative photo-physical, laser properties and molecular structures of three important Pyrromethene dyes, PM567, PM580 and PM597 show that all the three PM dyes are highly efficient. Particularly, PM597 dye produced a wider tuning range and lasing in a longer wavelength region, in spite of very low fluorescence yield and high non-radiative decay rate. A likely reason for observing the higher efficiency with PM dyes in comparison to RH6G dyes, are low GSA and presumably, low ESA of the PM dyes at the laser wavelengths. ESA, followed by rapid non-radiative relaxation to the excited laser level, acts as an intracavity photon loss mechanism that significantly reduces the laser efficiency. DFT/TDDFT calculations on ground and excited (S_1) states of all three PM dyes show a large distortion from the planarity of the two-pyrrole rings in the excited state of PM597 molecule. This, in turn, produced large Stokes shifts and presumably, low loss of laser photons due to GSA and ESA processes and thus make PM597 an efficient laser dye when used in laser cavity. Further studies to quantify GSA and ESA losses at pump and laser wavelengths of the dyes are required to understand the complex interplay between their molecular structures, photo-physical properties and laser performances. The longest wavelength absorption maximum of three PM dyes calculated by the DFT/TDDFT formalism are close to the experimental values, and could adequately reproduce the spectral shift induced by the different alkyl substitutions at C2 and C6 carbon positions of dyes along the long molecular axis. We plan to apply this theoretical combination (B3LYP/TDDFT + PCM solvent model) for calculating emission and other photo-physical properties of PM dyes for its utilization in designing new PM dye molecules having the desired photo-physical properties.

References

1. A. Loudet, K. Burgess, Chem. Rev. **107**, 4891 (2007)
2. G. Ulrich, R. Ziessel, A. Harriman, Angew. Chem. Int. Ed. **47**, 1184 (2008)
3. R.P. Haugland, in *Handbook of Fluorescence Probes and Research Products*, 9th edn., Molecular Probes, ed. by J. Gregory (Life Technologies, Berlin, 2002)
4. J.H. Boyer, A.M. Haag, G. Sathyamoorthi, M. Soong, K. Tangaraj, T.G. Pavlopoloulos, Heteroat. Chem. **4**, 39 (1993)
5. A. Costela, I. Gaecia-Marino, R. Sastre, in *Handbook of Advance Electronic and Photonic Materials Devices*, ed. by H.S. Nalwa (Academic Press, London, 1970)
6. W.P. Partridge, N.M. Laurendeau, C.C. Johnson, R.N. Steppel, Opt. Lett. **19**, 1630 (1994)
7. Y. Assor, Z. Burshtein, S. Rosenwaks, Appl. Opt. **41**, 1704 (2002)
8. I. Garcia-Moreno, F. Amat-Guerri, M. Liras, A. Costela, L. Infante, R. Sastre, F.L. Arbeloa, J.B. Prieto, I.L. Arbeloa, Adv. Funct. Mater. **17**, 3088 (2007)
9. G. Jones, O. Klueva, S. Kumar, D. Pacheco, Solid state laser X. Proc. SPIE **4267** (2001). doi:10.1117/12.424614
10. M.D. Rahn, T.A. King, A.A. Gorman, I. Hamblet, Appl. Opt. **36**, 5862 (1997)
11. A.K. Ray, S. Kundu, S. Sasikumar, C.S. Rao, S. Mula, S. Sinha, K. Dasgupta, Appl. Phys. B **87**, 483 (2007)
12. A. Costela, I. Garcia-Moreno, C. Gomez, R. Sastre, F. Amat-Guerri, M. Liras, F.L. Arbeloa, J.B. Prieto, I.L. Arbeloa, J. Phys. Chem. A **106**, 7736 (2002)
13. A. Costela, I. Garcia-Moreno, M. Pintado-Sierra, F. Amat-Guerri, M. Liras, R. Sastre, F.L. Arbeloa, J.B. Prieto, I.L. Arbeloa, J. Photochem. Photobiol. A **198**, 192 (2008)
14. S. Mula, A.K. Ray, M. Banerjee, T. Chaudhuri, K. Dasgupta, S. Chattopadhyay, J. Org. Chem. **73**, 2146 (2008)
15. J.B. Prieto, F.L. Arbeloa, V.M. Martinez, T.A. Lopez, I.L. Arbeola, J. Phys. Chem. A **108**, 5503 (2004)
16. H. Iikura, T. Tsuneda, T. Yanai, J. Hirao, Chem. Phys. **115**, 3540 (2001)
17. M. Henderson, A.F. Izmaylov, G.E. Scuseria, A. Savin, J. Chem. Phys. **127**, 221103 (2007)
18. M.A. Rohrdanz, J.M. Herbert, J. Chem. Phys. **129**, 34107 (2008)
19. M.A. Rohrdanz, K.M. Martins, J.M. Herbert, J. Chem. Phys. **130**, 054112 (2009)
20. K. Yagi, Y. Okano, T. Sato, Y. Kawashima, T. Tsuneda, K. Hirao, J. Phys. Chem. A **112**, 9845 (2008)
21. B.M. Wong, M. Piacenza, F.D. Sala, Phys. Chem. Chem. Phys. **11**, 4498 (2009)
22. A.K. Pathak, T. Mukherjee, D.K. Maity, J. Phys. Chem. A **114**, 721 (2010)
23. A.T.R. Williams, S.A. Winfield, J.N. Miller, Analyst **108**, 1067 (1983)
24. D. Jacquemin, E.A. Perpete, G.E. Scuseria, I. Ciofini, C. Adamo, J. Chem. Theory Comput. **4**, 123 (2008)
25. M.W. Schmidt, K.K. Baldridge, J.A. Boatz, S.T. Elbert, M.S. Gordon, J.H. Jensen, S. Koseki, N. Matsunaga, K.A. Nguyen, S.J. Su, T.L. Windus, M. Dupuis, J.A. Montgomery, J. Comput. Chem. **14**, 1347 (1993)
26. P.C. Beaumont, D.G. Jonson, B.J. Parsons, J. Chem. Soc. Faraday Trans. **89**, 4185 (1993)
27. J.M. Drake, R.I. Morse, R.N. Steppel, D. Young, Chem. Phys. Lett. **35**, 181 (1975)
28. J. Mohanty, K. Jagtap, A.K. Ray, W.M. Nau, H. Pal, Chem. Phys. Chem. **11** (2010). doi:10.1002/cphc.201000532